Structure, Dynamics, and Selectivity of the Sodium Channel Blocker μ-Conotoxin SIIIA[†,‡]

Shenggen Yao,[§] Min-Min Zhang,[||] Doju Yoshikami,[||] Layla Azam,[||] Baldomero M. Olivera,[||] Grzegorz Bulaj,[⊥] and Raymond S. Norton*[,§]

The Walter and Eliza Hall Institute of Medical Research, 1G Royal Parade, Parkville, Victoria 3050, Australia, Department of Biology, University of Utah, Salt Lake City, Utah 84112, and Department of Medicinal Chemistry, College of Pharmacy, University of Utah, Salt Lake City, Utah 84108

Received May 29, 2008; Revised Manuscript Received August 5, 2008

ABSTRACT: μ-SIIIA, a novel μ-conotoxin from *Conus striatus*, appeared to be a selective blocker of tetrodotoxin-resistant sodium channels in frog preparations. It also exhibited potent analgesic activity in mice, although its selectivity profile against mammalian sodium channels remains unknown. We have determined the structure of μ-SIIIA in aqueous solution and characterized its backbone dynamics by NMR and its functional properties electrophysiologically. Consistent with the absence of hydroxyprolines, μ-SIIIA adopts a single conformation with all peptide bonds in the trans conformation. The C-terminal region contains a well-defined helix encompassing residues 11−16, while residues 3−5 in the N-terminal region form a helix-like turn resembling 3_{10}-helix. The Trp12 and His16 side chains are close together, as in the related conotoxin μ-SmIIIA, but Asn2 is more distant. Dynamics measurements show that the N-terminus and Ser9 have larger-magnitude motions on the subnanosecond time scale, while the C-terminus is more rigid. Cys4, Trp12, and Cys13 undergo significant conformational exchange on microsecond to millisecond time scales. μ-SIIIA is a potent, nearly irreversible blocker of $Na_V1.2$ but also blocks $Na_V1.4$ and $Na_V1.6$ with submicromolar potency. The selectivity profile of μ-SIIIA, including poor activity against the cardiac sodium channel, $Na_V1.5$, is similar to that of the closely related μ-KIIIA, suggesting that the C-terminal regions of both are critical for blocking neuronal $Na_V1.2$. The structural and functional characterization described in this paper of an analgesic μ-conotoxin that targets neuronal subtypes of mammalian sodium channels provides a basis for the design of novel analogues with an improved selectivity profile.

Toxins from the genus *Conus* are valuable tools in elucidating the physiological functions of their targets and in probing the size and shape of their cognate binding sites (*1, 2*). Conotoxins that target voltage-gated sodium channels (VGSCs),[1] which are responsible for the influx of sodium ions during action potentials in excitable tissues, represent a particularly good example. Four families of conotoxins target these channels, causing activation (ι-conotoxins), inhibition (μ- and μO-conotoxins), or inhibition of fast inactivation (δ-conotoxins). Among the most extensively studied of these in terms of their interactions with the channel are the μ-conotoxins. These toxins bind to site 1 on VGSCs (*3*), which is located on the extracellular surface of the pore-forming α-subunit and also binds guanidinium alkaloids tetrodotoxin (TTX) and saxitoxin. Of the nine α-subunits cloned from mammals (*4, 5*), six bind TTX with high affinity (IC_{50} in the nanomolar range), and three, $Na_V1.5$, $Na_V1.8$, and $Na_V1.9$, are classified as TTX-resistant (IC_{50} > 1 μM).

The first μ-conotoxin characterized, μ-GIIIA, targets mainly the skeletal muscle subtype $Na_V1.4$ (*6*−*9*). μ-PIIIA also has a strong preference for $Na_V1.4$ but can block other TTX-sensitive subtypes as well, albeit with lower affinities (*8, 10, 11*). Recently, a new group of μ-conotoxins was discovered that targets neuronal sodium channels with greater selectivity and potency than μ-GIIIA or μ-PIIIA (*12*−*16*). This group includes μ-SmIIIA, which irreversibly inhibited TTX-resistant sodium currents in amphibian sympathetic and dorsal root ganglion (DRG) neurons (*12*), as well as μ-KIIIA and μ-SIIIA (*14*). The selectivity of these new μ-conotoxins toward mammalian sodium channel subtypes was defined only recently, when it was shown that μ-KIIIA was a potent blocker of the neuronal subtype $Na_V1.2$ and that several amino acid residues, including Lys7 and His12, were critical for activity (*15*). Thus, the new group of μ-conotoxins

[†] This work was supported in part by National Institute of General Medical Sciences Grant GM 48677 (to B.M.O.). R.S.N. acknowledges fellowship support from the Australian National Health and Medical Research Council.

[‡] Chemical shift assignments and the family of structures for μ-SIIIA have been deposited in the BioMagResBank under accession number 20023.

* To whom correspondence should be addressed: The Walter and Eliza Hall Institute of Medical Research, 1G Royal Parade, Parkville, Victoria 3050, Australia. Phone: +61 3 9345 2306. Fax: +61 3 9345 2686. E-mail: ray.norton@wehi.edu.au.

[§] The Walter and Eliza Hall Institute of Medical Research.

[||] Department of Biology, University of Utah.

[⊥] Department of Medicinal Chemistry, University of Utah.

[1] Abbreviations: μ-GIIIA and μ-GIIIB, μ-conotoxins GIIIA and GIIIB, respectively, from *Conus geographus*; μ-KIIIA, μ-conotoxin KIIIA from *Conus kinoshitai*; μ-PIIIA, μ-conotoxin PIIIA from *Conus purpurascens*; μ-SIIIA, μ-conotoxin SIIIA from *Conus striatus*; μ-SmIIIA, μ-conotoxin SmIIIA from *Conus stercusmuscarum*; MD, molecular dynamics; rms, root-mean-square; TTX, tetrodotoxin; VGSC, voltage-gated sodium channel.

10.1021/bi801010u CCC: $40.75
Published on Web 09/18/2008

consisting of μ-KIIIA, μ-SIIIA, and μ-SmIIIA is a promising source of subtype-selective blockers of neuronal sodium channels.

Relatively little is known about the biological activity or structural properties of μ-SIIIA. μ-SIIIA was shown to potently block TTX-insensitive sodium currents in amphibian DRG and sympathetic ganglion neurons, but it was a relatively poor inhibitor of TTX-sensitive channels in frog skeletal muscle preparations (*12*). Micromolar concentrations of μ-SIIIA slowly blocked TTX-sensitive currents in mouse DRG neurons, and 1 μM peptide almost completely blocked A-compound action potentials in mouse sciatic nerve preparations after exposure for 1 h (*17*). μ-SIIIA appeared to significantly reduce the acute and inflammatory pain responses in the formalin assay in mice at doses of <1 mg/kg following intraperitoneal administration (*17*). These results strongly suggested that μ-SIIIA has therapeutic potential as a potent blocker of mammalian sodium channels, but the subtype selectivity or structural properties of this μ-conotoxin remain unknown.

Previous NMR studies of μ-conotoxins have found evidence of conformational flexibility, manifested in line broadening of one or more resonances (*18*−*20*), although this was not the case for μ-SmIIIA (*13*). However, when μ-SmIIIA was subjected to molecular dynamics simulations, the resulting structure exhibited several differences from the one calculated on the basis of NMR restraints (*14*). In particular, the side chain of Arg2 moved away from that of Trp14, in conflict with the observed NOEs between these side chains (*13*), and the first loop (between Asn5 and Gly9) sampled a larger region of conformational space than in the NMR structure. Apart from these differences, the rest of the backbone was largely constant throughout the simulation and consistent with the NMR structure. Nonetheless, these observations raise questions about the flexibility of μ-conotoxin structures, which are germane to their use as a basis for modeling new structures in this superfamily and for the design of nonpeptidic mimetics (*17*).

NMR relaxation measurements provide a means of characterizing protein solution dynamics over a broad range of time scales. Experimental procedures for measuring ^{15}N relaxation parameters (R_1, R_2, and steady-state $^{15}N-\{^1H\}$ NOE) as well as protocols for data analysis using Modelfree formalism are well established for the study of protein backbone dynamics on picosecond to nanosecond time scales (*21, 22*). There is also compelling evidence that protein dynamics in solution, particularly on the millisecond time scale, correlate closely with protein function (*23*−*25*). This is significant because one of the mechanisms underlying protein function and protein−protein interaction is conformational exchange, which typically occurs on the submillisecond to millisecond time scales (*26*).

Most of these studies have been conducted using isotopically enriched proteins produced in bacteria grown on minimal media. Toxins with multiple disulfide linkages such as the μ-conotoxins can be expressed and isotopically labeled in heterologous expression systems (*27*), but most toxins that are the subject of structural studies are produced by solid-phase synthesis without labeling. With the widespread availability of NMR cryoprobes, it has become straightforward to obtain ^{13}C and ^{15}N chemical shifts for unlabeled samples (*28, 29*), and these parameters are useful in defining backbone and potentially also side chain dihedral angles (*30*). Given that ^{13}C has a higher natural abundance and sensitivity than ^{15}N (1.11 and 0.37%, respectively, and sensitivities for the same number of nuclei relative to ^1H of 1.59×10^{-2} and 1.04×10^{-3}, respectively), it has also become feasible to monitor ^{13}C relaxation on unlabeled samples. In the past, this has required large sample tubes and/or concentrated samples (e.g., refs *31* and *32*), but such studies can now be undertaken in a reasonable time with ~1 mM samples. In this paper, we describe the results of a ^{13}C NMR relaxation study of the conotoxin μ-SIIIA, which was undertaken to determine whether such measurements could detect internal motions in this class of toxins on time scales relevant to conformational averaging and biological activity. To interpret the relaxation data, we have also determined a high-resolution structure for μ-SIIIA and compared it with the structures of other μ-conotoxins.

EXPERIMENTAL PROCEDURES

Peptide Synthesis and Sample Preparation. μ-SIIIA used for the structural and functional characterization described here was synthesized chemically using the protocols described previously (*14*). The oxidative folding of μ-SIIIA readily yielded a single folded species in the presence of oxidized and reduced glutathione (*14, 17*); this form was purified using C18 reversed-phase HPLC, and its identity was confirmed by mass spectrometry. Samples used for structure determination and ^{13}C relaxation measurements were prepared by dissolving μ-SIIIA in 350 μL of a 95% H_2O/5% ^2H_2O mixture or 100% ^2H_2O to a final concentration of approximately 0.9 mM. The pH was adjusted to 4.2 without allowance for isotope effects.

NMR Spectroscopy. For structure determination, two-dimensional (2D) TOCSY (spin-lock time of 60 ms), NOESY (mixing time of 250 ms), and DQF-COSY spectra were recorded on a Bruker DRX600 spectrometer at 25 °C. Complex data matrices of 2048 × 225 points for TOCSY, 2048 × 300 points for NOESY, and 2048 × 300 points for DQF-COSY and 40,112, and 40 scans per t_1 increment in the indirect detected dimension were used. Assignments of aliphatic carbon resonances were established from ^{13}C HSQC, ^{13}C HMQC, and ^{13}C HMQC-TOCSY (*33*) spectra, whereas backbone ^{15}N resonances of μ-SIIIA were assigned from a ^{15}N HSQC spectrum on the basis of the corresponding amide proton chemical shifts, which were well-resolved in the F_2 (^1H) dimension. All of these heteronuclear correlation spectra were recorded at natural abundance on a Bruker Avance500 instrument using a TXI cryoprobe. ^{13}C R_1, R_2, and $^{13}C-\{^1H\}$ NOEs were also measured at natural abundance on the Bruker Avance500 instrument at 283, 298, and 310 K using standard pulse sequences in the Bruker pulse sequence library. Relaxation-weighted ^{13}C HSQC spectra were acquired in an interleaved manner; i.e., a three-dimensional (3D) data set was acquired with the pulse sequence stepping through the relaxation durations prior to signal averaging and the time increments of the indirectly detected dimension of the spectra. Twelve relaxation delays, including two duplicated delays, ranging from 10 to 800 ms for R_1 and from 22.4 to 268.8 ms for R_2 were measured. A complex data matrix of 2048 × 32 points together with 48 scans per t_1 increment for R_1 and R_2 and 192 for the NOE

were used. The recycle times were 2.8 s for R_1 and R_2 and 4.0 s for the steady-state $^{13}C-\{^1H\}$ NOE. All NMR spectra were processed using TOPSPIN (version 1.3, Bruker BIOSPIN) and analyzed using XEASY version 1.3 (*34*).

Structure Calculations. Volumes of cross-peaks in a 250 ms mixing time NOESY spectrum recorded at 25 °C were converted to distance restraints using the script CALIBA supplied with CYANA (*35*). The resultant values were then scaled by a factor of 1.2 to allow for potential effects of spin diffusion. Pseudodistance restraints of 3.0 Å for $C^\beta-S^\gamma$ bonds and 2.0 Å for $S^\gamma-S^\gamma$ bonds were added for all three disulfide bonds [Cys3−Cys13, Cys4−Cys19, and Cys8−Cys20, based on sequence alignment with closely related μ-conotoxins (*13, 14*)]. Backbone ϕ angle restraints were derived from $^3J_{HNNA}$ coupling constraints measured from the DQF-COSY spectrum ($^3J_{HNH\alpha} > 8$ Hz, $\phi = -120 \pm 30°$; $^3J_{HNH\alpha} < 6$ Hz, $\phi = -60 \pm 30°$) and combined with those derived from TALOS (*30*) on the basis of chemical shifts of N, H^α, C^α, and C^β atoms of μ-SIIIA. All other residues were restricted to a negative ϕ value except for Gly6 and Gly7, which were not restrained. Initial structures were generated using the torsion angle dynamics program CYANA (*35*) for refinement of structural restraints. The final distance and angle restraints were then used to calculate a family of 400 structures in XPLOR-NIH (*36*) using standard distance geometry and simulation annealing scripts. Residue pyroGlu was added into the XPLOR library as previously described (*13*). A group of 50 structures out of those 400 calculated structures with lowest NOE energies was then further refined using simulated annealing. The resultant structures were further refined in a water box built around the peptide and then energy minimized on the basis of experimental distance and angular restraints as well as the geometry of bonds, angles, and improper angles. A family of 20 structures, based on their stereochemical energies and NOE energies, was then chosen for structural analysis using PROCHECK (*37*) and MOLMOL (*38*). This family of final structures and associated structural restraints have been deposited in the BioMagResBank (*39*) under accession number 20023.

Analysis of ^{13}C Relaxation Data. ^{13}C relaxation rates R_1 and R_2 were obtained by fitting peak intensities at a series of relaxation durations to a two-parameter single-exponential decay curve using SigmaPlot. Errors in the relaxation rates were standard deviations from fittings in SigmaPlot. The steady-state $^{13}C-\{^1H\}$ NOE values were calculated from peak intensity ratios obtained from spectra acquired in the presence and absence of proton saturation with uncertainties of 5% for peak intensities determined from the background noise of the spectra (*40*).

^{13}C relaxation parameters were first analyzed using Modelfree formalism. Given that the rotational correlation time of μ-SIIIA is in the low nanosecond range, fittings to the extended spectral density function, which includes a slower time scale of internal motion, were not attempted. ^{13}C R_1, R_2, and NOE values were fitted to one of three models [(1) S^2, (2) S^2 and τ_e, and (3) S^2 and R_{ex}] using criteria similar to those of the model selection approach commonly used in ^{15}N relaxation analysis (*41*).

In contrast to Modelfree analysis, reduced spectral density mapping extracts information about molecular dynamics without approximations made regarding molecular shape and global rotational behavior. While reduced spectral density mapping has been commonly used in the analysis of backbone ^{15}N relaxation data, it is more limited for ^{13}C relaxation data than for ^{15}N. It has been noted previously that, while reduced spectral density mapping introduced few errors for ^{15}N relaxation analysis, it was less valid for ^{13}C as the derivation of reduced spectral density functions (eqs 1b and 1c) assuming spectral density function $J(\omega)$ is flat around ω_H; i.e., $J(\omega_H - \omega_N) = J(\omega_H) = J(\omega_H + \omega_N)$ for ^{15}N, and $J(\omega_H - \omega_C) = J(\omega_H) = J(\omega_H + \omega_C)$ for ^{13}C (*42*). Nevertheless, it provides a picture of the local dynamics of the molecule complementary to that obtained from Modelfree analysis, provided the value for $J(1.563\omega_H)$ is not interpreted (*43*).

The values of spectral density functions $J(0)$, $J(\omega_C)$, and $J(1.563\omega_H)$ were calculated from measured ^{13}C R_1, R_2, and steady-state NOE values similar to those described previously for reduced spectral density mapping of ^{15}N relaxation parameters.

$$\sigma_{C\alpha H} = R_1(\mathrm{NOE} - 1)\gamma_C/\gamma_H \quad (1a)$$

$$J(0) = (6R_2 - 3R_1 - 2.72\sigma_{C\alpha H})/(3d^2 + 4c^2) \quad (1b)$$

$$J(\omega_C) = (4R_1 - 5\sigma_{C\alpha H})/(3d^2 + 4c^2) \quad (1c)$$

$$J(1.563\omega_H) = 4\sigma_{C\alpha H}/(5d^2) \quad (1d)$$

where $d = [\mu_0 h\gamma_C\gamma_H/(8\pi^2)]/\langle r_{C\alpha H}{}^3\rangle$, $c = \omega_C(\sigma_{||} - \sigma_\perp)/3^{1/2}$, μ_0 is the permeability of free space, h is Planck's constant, γ_H and γ_C are the gyromagnetic ratios of ^1H and ^{13}C, respectively, $r_{C\alpha H}$ (=1.09 Å) is the average amide bond length, and $\sigma_{||} - \sigma_\perp$ (=25 ppm) is the chemical shift anisotropy for $^{13}C^\alpha$ nuclei (*44*).

Electrophysiology of Mammalian Na_V Clones Expressed in Xenopus Oocytes. Oocytes expressing VGSCs were prepared and two-electrode voltage-clamped essentially as described previously (*15, 45*). Briefly, oocytes were placed in a 30 μL chamber containing ND96 and two-electrode voltage-clamped with a holding potential of −80 mV. To activate Na channels, the membrane potential was stepped to a value between −20 and 0 mV (depending on the Na_V subtype) for a period of 50 ms every 20 s. To apply toxin, we halted the perfusion, applied 3 μL of toxin solution (at 10 times the final concentration) to the 30 μL bath, and manually stirred the bath for ~5 s by gently aspirating and expelling a few microliters of the bath fluid several times with a micropipette. Toxin exposures were in static baths to conserve material. On-rate constants were obtained from the slopes of k_{obs} versus peptide concentration, where k_{obs} was determined from the single-exponential fit of the time course of block by a given toxin concentration. Off-rate constants were determined from single-exponential fits of the time course of recovery from block following toxin washout. All recordings were taken at room temperature (~21 °C).

RESULTS

Chemical Shift Assignments. A one-dimensional ^1H NMR spectrum of μ-SIIIA in aqueous solution (Figure S1 of the Supporting Information) showed a single major species with good spectral dispersion. Chemical shift assignments were obtained for resonances from all amide and aliphatic ^1H, aliphatic ^{13}C, and backbone ^{15}N atoms of μ-SIIIA. These assignments have been deposited in the BioMagResBank

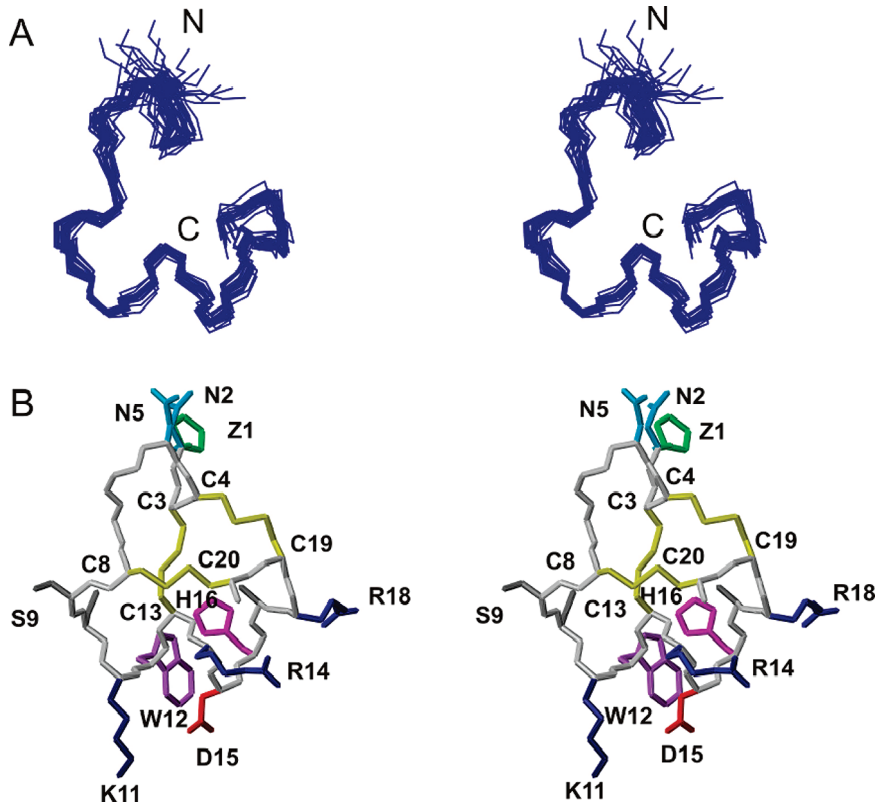

FIGURE 1: μ-SIIIA structure. (A) Stereoview of backbone μ-SIIIA [a family of 20 final solution structures of μ-SIIIA superimposed over backbone heavy atoms (N, C^{α}, and C′) of all 20 residues]. The letters N and C refer to the N- and C-termini, respectively. (B) Stereoview of closest-to-mean structure in the family of 20 structures shown in panel A with the backbone of μ-SIIIA colored light gray and side chains of several residues highlighted in color. Those residues with side chains highlighted are also labeled. The three disulfide bonds (Cys3−Cys13, Cys4−Cys19, and Cys8−Cys20) are colored yellow.

(accession number 20023) and are tabulated in the Supporting Information (Table S1). Plots of secondary chemical shifts of backbone H^N, N, C^{α}, and H^{α} atoms versus the sequence of μ-SIIIA are shown in Figure S2 of the Supporting Information; the H^{α} and C^{α} shifts for residues 11−16 are consistent with the presence of α-helical structure in this region of the molecule.

Solution Structure. Parameters characterizing the final 20 structures of μ-SIIIA and structural statistics are summarized in Table 1. The final 20 structures fit well with experimentally derived distance and angle constraints and are well defined over the entire length of the polypeptide, with the N-terminal pyroGlu1 and Asn2 residues being slightly less ordered than the rest of the polypeptide chain. A summary of backbone rms deviations and backbone angular order parameters (*46, 47*) of μ-SIIIA is shown in Figure S4 of the Supporting Information, and stereoviews of the structures are shown in Figure 1.

The main secondary structure element is a well-defined C-terminal helix (residues 11−16), but N-terminal residues 3−5 also appear to form a helixlike turn resembling 3_{10}-helix. The side chain of Lys11, which may be important for binding to site 1 on VGSC in μ-SIIIA, is only partially exposed because of its proximity to the side chains of Trp12 and Asp15.

^{13}C Relaxation Parameters and Rotational Correlation Times. After Gly6 and Gly7 had been excluded, as well as residues whose measurements were compromised by the residual water resonance in the directly detected dimension (F_2), ^{13}C R_1, R_2, and $^{13}C-\{^1H\}$ NOE values were measured for a total of 15, 16, and 16 C^{α} atoms of μ-SIIIA at 283, 298, and 310 K, respectively, as shown in Figure 2. A $^{13}C-^1H$ HSQC spectrum of μ-SIIIA at 298 K, representative decay curves of R_1 and R_2, and all measured $^{13}C^{\alpha}$ relaxation parameters are given in the Supporting Information (Figures

Table 1: Structural Statistics for μ-SIIIA in Aqueous Solution at 298 K

no. of distance restraints	164
intra ($i = j$)	53
sequential ($\|i - j\| = 1$)	68
short ($1 < \|i - j\| < 6$)	31
long	12
no. of dihedral restraints	22
energy (kcal/mol)[a]	
E_{NOE}	7.5 ± 0.8
deviations from ideal geometry[b]	
bonds (Å)	0.0065 ± 0.0002
angles (deg)	0.743 ± 0.014
impropers (deg)	0.551 ± 0.021
rms deviation (Å)[c]	
all heavy atoms	1.22
backbone heavy atoms (N, C^{α}, and C′)	0.74
average pairwise rms deviation	
all heavy atoms	1.83 ± 0.43
backbone heavy atoms (N, C^{α}, and C′)	1.06 ± 0.36
Ramachandran plot[d]	
most favored (%)	91.6
allowed (%)	8.4
additionally allowed (%)	0
disallowed (%)	0

[a] The values for E_{NOE} are calculated from a square well potential with force constants of 50 kcal mol^{-1} $Å^2$. [b] The values for the bonds, angles, and impropers show the deviations from ideal values based on perfect stereochemistry. [c] The rmsd over the backbone heavy atoms (N, C^{α}, and C) of all residues. [d] As determined with PROCHECK-NMR (*37*) for all residues except Gly and Pro.

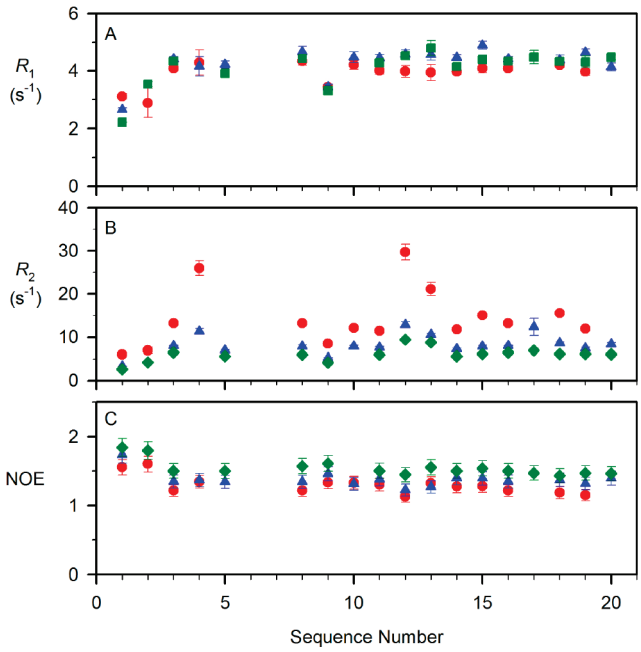

FIGURE 2: C^{α} ^{13}C relaxation parameters, R_1, R_2, and NOE, of μ-SIIIA measured at 283 (●), 298 (▲), and 310 K (◆). Data are not shown for Gly6 and Gly7, and residues whose resonances lay too close to the residual water resonance in the F_2 dimension (Figure S5 and Table S2 of the Supporting Information).

S5 and S6 and Table S2). The average values of R_1, R_2, and NOE as well as effective rotational correlation times of μ-SIIIA estimated from the average ^{13}C R_2/R_1 ratio (residues with angular order parameters S_ϕ and S_ψ > 0.9 and their R_2/R_1 values within one standard deviation of the averaged R_2/R_1 ratio) are listed in Table 2. The rotational correlation time of μ-SIIIA from hydrodynamics calculations based on its closest-to-mean structure is also shown.

Dynamics Parameters. Dynamics parameters of μ-SIIIA resulting from Modelfree analysis and reduced spectral density mapping from its $^{13}C^{\alpha}$ relaxation parameters measured at 283, 298, and 310 K are summarized in Figures 3 and 4, respectively, and tabulated in the Supporting Information (Tables S3 and S4). Average S^2 values over the entire molecule (from residues with S^2 values available at all three temperatures) and over the C-terminal helical region (residues 11 −16) are also summarized in Table 2.

Temperature Dependence of Dynamics Parameters. The observed decrease in order parameters at higher temperatures reflects increased amplitudes of motion of the C^{α}−H bond vectors, with several residues (Cys8 and Ser9, and to a lesser extent Lys11, Arg14, and Asp15) exhibiting a more pronounced temperature dependence than the average over the entire polypeptide chain or the C-terminal helical region (residues 11−16) (Figure 3). Figure 5 summarizes the temperature dependence of the order parameters (shown as $1 - S$) of μ-SIIIA for the average over the entire molecule, the C-terminal helical region, Ser9, and Lys11 (Figure 5A), as well as the temperature dependence of apparent chemical exchange, R_{ex}, for Cys4, Trp12, and Cys13 (Figure 5B). Ribbon presentations of μ-SIIIA with its structural characteristics and dynamics parameters highlighted are shown in Figure 6.

Functional Studies. The activity of μ-SIIIA on cloned α-subunits of rat (r) or mouse (m) sodium channels expressed in oocytes was assessed by voltage-clamp protocols. Table 3 summarizes dose-dependent inhibition by μ-SIIIA of seven sodium channel subtypes, including skeletal muscle $rNa_V1.4$ and heart muscle $rNa_V1.5$. Four neuronal subtypes, $rNa_V1.1$, $rNa_V1.2$, $rNa_V1.3$, and $mNa_V1.6$, were blocked by μ-SIIIA with IC_{50} values ranging from <0.76 to 11 μM. The block of $rNa_V1.2$ was only very slowly reversible (Figure 7); in contrast, the block of $rNa_V1.1$, $rNa_V1.3$, and $mNa_V1.6$ was readily reversible. Of the channels that were tested, $rNa_V1.4$ was blocked with the fastest on-rate and second slowest off-rate. Inhibition of $rNa_V1.5$ and $rNa_V1.7$ was characterized by a very low affinity, with IC_{50} values of 251 and 65 μM, respectively. Of the five IC_{50} values determined in Table 3, the corresponding K_d values (calculated from k_{off}/k_{on}) for four were within a factor of 2. For $Na_V1.7$, however, the K_d (15 μM) was 4-fold lower than the IC_{50}; we attribute this discrepancy to the fact that the block of $Na_V1.7$ had the slowest on-rate and a relatively slow off-rate, which created a long period for reaching the steady state and therefore a less reliable determination of IC_{50}.

DISCUSSION

Conotoxins μ-SmIIIA, μ-KIIIA, and μ-SIIIA are potent sodium channel blockers; indeed, the latter two were shown recently to possess potent analgesic activity in the inflammatory pain assay in mice (*15, 17*). μ-KIIIA and μ-SIIIA share a high degree of sequence homology in the C-terminal part of their structure. Consistent with this, the selectivity profile of μ-SIIIA for the various Na_V subtypes was similar to that described previously for μ-KIIIA (*15*). Both were nearly irreversible blockers of $Na_V1.2$ and reversible blockers of skeletal muscle subtype $Na_V1.4$. However, neuronal subtype $Na_V1.7$ was more readily blocked by μ-KIIIA [K_d = 0.29 μM (*15*)] than by μ-SIIIA (IC_{50} = 65 μM or K_d = 15.0 μM; see Table 3 and the last paragraph of Results), suggesting that either Ser13 in μ-KIIIA is an important determinant of the interactions with $Na_v1.7$ (the homologous residue in μ-SIIIA is Ala17) or some minor conformational differences between the two peptides may be responsible for their different potencies. In any event, our current functional data suggest that the N-terminal region of μ-conotoxins SIIIA, KIIIA, and SmIIIA is important for determining subtype selectivity in these peptides, whereas the C-terminal region contains a common pharmacophore for interactions with the neuronal subtypes of sodium channels.

Comparison with Structures of μ-SmIIIA and Other μ-Conotoxins. The structures of several μ-conotoxins have been determined previously, including μ-SmIIIA [PDB entry 1Q2J (*13*)], μ-PIIIA [PDB entry 1R9I (*11*)], μ-GIIIA [PDB entry 1TCJ (*19*)], and μ-GIIIB [PDB entry 1GIB (*20*)]. A sequence alignment of these μ-conotoxins is shown in Figure 8 along with a comparison of their structures. Superposition of these five structures over their C-terminal halves is significantly better than that over their N-terminal halves (Figure 8B). As noted by Keizer et al. (*13*), this is at least partly a consequence of the trans conformation for the peptide bond preceding residue 8 in μ-SmIIIA and the major form of μ-PIIIA, as opposed to the cis conformation in μ-GIIIA, μ-GIIIB, and the minor form of μ-PIIIA. All peptide bonds in μ-SIIIA are also in the trans conformation. The C-terminal region of μ-SIIIA contains a well-defined helix (residues 11−16), and the N-terminal region contains a helix-like turn resembling 3_{10}-helix at residues 3−5.

Table 2: Summary of Average ^{13}C Relaxation Parameters, Rotational Correlation Times, and Order Parameters of μ-SIIIA

T (K)	$\langle R_1 \rangle$ (s^{-1})	$\langle R_2 \rangle$ (s^{-1})	⟨NOE⟩	$\langle R_2/R_1 \rangle^a$	τ_c (ns)	$\tau_c'^b$ (ns)	$\langle S^2 \rangle^c$ (overall)	$\langle S^2 \rangle^d$
283	3.91 ± 0.43	14.38 ± 6.59	1.30 ± 0.13	3.04 ± 0.41 (11/15)	2.29 ± 0.25	2.72	0.91 ± 0.17	0.97 ± 0.01
298	4.28 ± 0.54	8.07 ± 2.20	1.38 ± 0.11	1.87 ± 0.43 (16/16)	1.45 ± 0.19	1.80	0.80 ± 0.21	0.85 ± 0.02
310	4.12 ± 0.63	6.06 ± 1.59	1.54 ± 0.12	1.45 ± 0.22 (16/16)	0.98 ± 0.15	1.32	0.76 ± 0.20	0.84 ± 0.07

[a] Average value over residues whose R_2/R_1 were within 1.5 standard deviations of the averaged value of R_2/R_1 of all measured residues; the number of residues that satisfies the criteria vs the total number of residues whose ^{13}C relaxation parameters are measured is given in parentheses. [b] Effective rotational correlation times of μ-SIIIA from hydrodynamic calculation, using HYDRONMR with a radius of atomic elements of 3.1 Å and viscosities of 100% ^2H_2O. Previously published values of viscosities for 100% ^2H_2O of 1.679×10^{-3}, 1.110×10^{-3}, and 0.850×10^{-3} N s m^{-2} at 283, 298, and 310 K, respectively, were used (*55*). [c] Averaged over a group of 12 residues with order parameters determined at all three temperatures. [d] Average value over the helical region (residues 11−16).

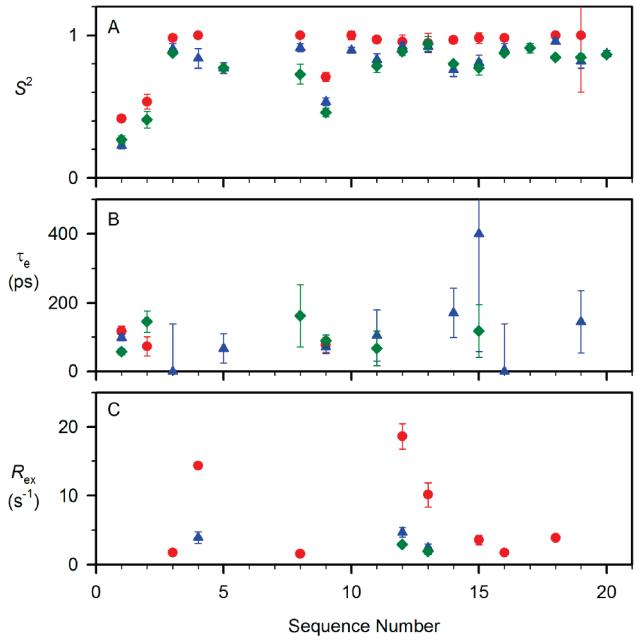

FIGURE 3: Dynamics parameters of μ-SIIIA. (A) S^2, (B) τ_e, and (C) R_{ex} at 283 (●), 298 (▲), and 310 K (◆) derived from ^{13}C C^α relaxation parameters shown in Figure 2 using the Modelfree formalism.

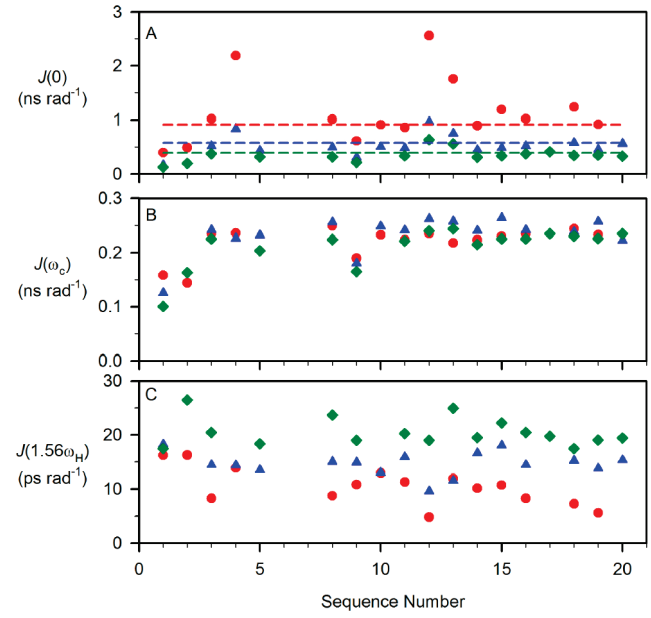

FIGURE 4: Reduced spectral density functions of μ-SIIIA. (A) $J(0)$, (B) $J(\omega_C)$, and (C) $J(1.563\omega_H)$ at 283 (●), 298 (▲), and 310 K (◆) calculated from ^{13}C relaxation parameters depicted in Figure 2 using eqs 1a−1d. Dashed lines in panel A corresponding to $(^2/_5)\tau_c$, indicating $J(0)$ values for a completely rigid molecule at the given rotational correlation times (283 K in red, 298 K in blue, and 310 K in green for μ-SIIIA).

In μ-SmIIIA, the indole ring of Trp14 is flanked by the imidazolium ring of His18 on one side and the guanidinium moiety of Arg2 on the other (*13*), these side chain interactions presumably being favored not only by interactions between the π orbitals of the indole and imidazolium rings but also by aromatic−cation interactions. The equivalent Trp in μ-SIIIA, Trp12, is also close to His16 (Figure 1B), but these residues are some distance from residue 2, which is Asn in μ-SIIIA. The $H^{\delta 2}$ resonance of His16 of μ-SIIIA has a chemical shift very similar to that of His18 in μ-SmIIIA (Table S1), implying that it is influenced by ring current shifts from the Trp indole ring as a consequence of their proximity in both structures. Analysis of ring current shifts on the final family structures of μ-SIIIA performed using MOLMOL (*38*) resulted in very similar upfield shifts for resonances from $C^\alpha H$, $C^\beta H$, and the ring protons of His16, as previously reported for His18 in μ-SmIIIA (*13*).

Comparison with Model Structure. Models of both μ-SIIIA and μ-KIIIA were generated in the course of MD simulations performed to gain insight into the potential structural consequences of deleting a number of residues in the first loop (the region flanked by the second and third Cys residues) (*14*). Figure S7 of the Supporting Information compares stereoviews of the μ-SIIIA model with our solution structure. The C-terminal halves of the two are very similar (backbone rmsd of 1.07 Å for residues 11−20, compared with 2.58 Å for residues 1−10), and the helical region (residues 11−16) is conserved. The difference seen in the N-terminal region may be attributed to apparent structural differences between μ-SIIIA and μ-SmIIIA, as the model structure of μ-SIIIA was generated on the basis of the reported structure of μ-SmIIIA. As described in the introductory section, the simulated structure of μ-SmIIIA showed several differences from the structure determined from NMR data (*13*).

Backbone Dynamics of μ-SIIIA. Reduced flexibility is observed for μ-SIIIA at lower temperatures, as reflected in its overall S^2 (Figure 3A) and $J(0)$ values (Figure 4A). Relatively lower S^2 values compared with the average over the entire backbone were observed for pyroGlu1, Asn2, and Ser9. The angular order parameters S_ϕ and S_Ψ (Figure S3 of the Supporting Information) also show relatively lower values for pyroGlu1 and Asn2 but not for Ser9. It appears that the N-terminus shows larger-magnitude motions on the sub-nanosecond time scale, while the C-terminus is more rigid, although the difference is small if the first two residues are ignored. As disulfide bridges connect Cys3 and Cys4 to the C-terminal half of the molecule, there is no simple correlation between the locations of the disulfides and relative backbone flexibility. Greater flexibility is anticipated near the chain termini, which is in accord with our observations for residues

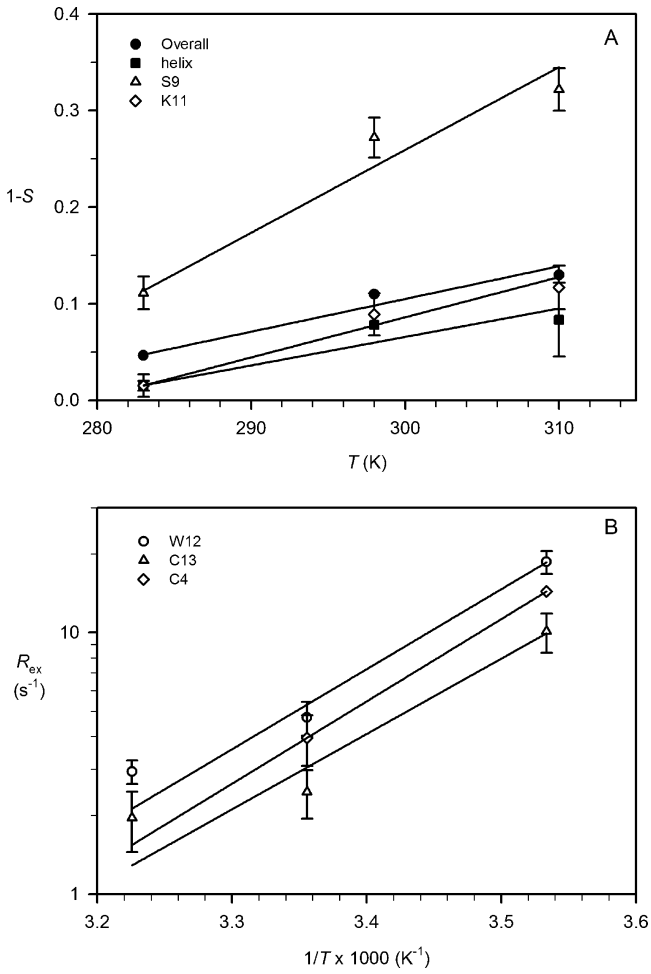

FIGURE 5: Temperature dependence of chemical exchange and order parameters for μ-SIIIA. (A) Order parameters are shown as $1 - S$ vs T for (●) the average value of the overall sequence (12 residues with S^2 values at all three temperatures were determined), (■) the C-terminal helix (residues 11−16), (△) Ser9, and (◇) Lys11. (B) Temperature dependence of chemical exchange shown as an Arrhenius plot (ln R_{ex} vs $1/T$) for resides Cys4 (◇), Trp12 (○), and Cys13 (△).

1 and 2, but the C-terminal residue, Cys20, participates in a disulfide bond and has S^2 values essentially identical with those of other residues in the C-terminal half. The only other residue to exhibit greater motion on the subnanosecond time scale is Ser9 (Figure 3A), which is located in the middle of the polypeptide chain and adjacent to Cys8.

Conformational Exchange of μ-SIIIA Motion on Microsecond to Millisecond Time Scales. Larger $J(0)$ values were observed for the backbone at 283 K compared with 298 and 310 K, indicating reduced subnanosecond motions of the C^{α}−H bond vectors at lower temperatures (Figure 4A). Slower microsecond to millisecond motions due to conformational exchange experienced by backbone C^{α} atoms may also be reflected in the spectral density function at angular frequency, $\omega = 0$, which give rise to elevated values for $J(0)$. For μ-SIIIA, significantly higher $J(0)$ values were observed for Cys4, Trp12, and Cys13 at 283 K, which agrees very well with the result from Modelfree analysis that significant apparent R_{ex} terms are needed to fit the relaxation data of these residues (Figure 3C).

The interpretation of R_{ex} in terms of chemical or conformational exchange contributions to the transverse relaxation

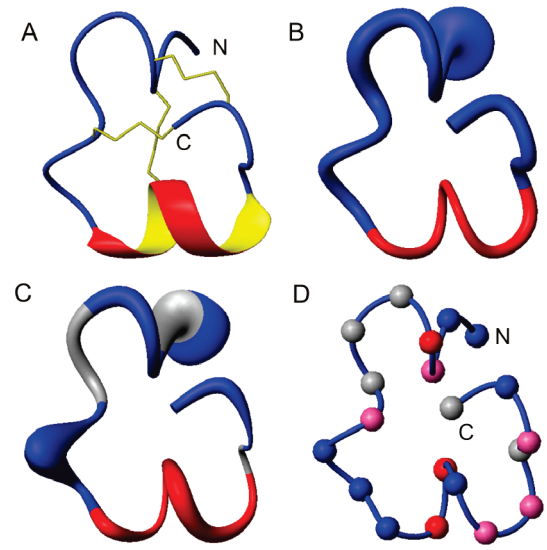

FIGURE 6: (A) Ribbon diagram of μ-SIIIA (closest-to-mean) with three disulfide bridges (Cys3−Cys13, Cys4−Cys19, and Cys8−Cys20) highlighted in yellow. (B) Mean structure of the final family of 20 structures of μ-SIIIA (BioMagResBank accession number 20023) with radii of backbone atoms proportional to their averaged displacement from the mean structure. Note that this structure is not the same as that shown in panels A, C, and D. (C) Ribbon diagram of SIIIA (closest-to-mean) with radii of backbone atoms proportional to $1 - S^2$, where S^2 is the order parameter that resulted from Modelfree analysis of $^{13}C^{\alpha}$ relaxation parameters measured at 298 K (Figure 3). Residues 2, 6, 7, and 17, whose S^2 values were not determined, are colored gray with their bond radii shown as the averaged values from their neighboring residues. (D) Backbone C^{α} atoms of μ-SIIIA, shown as spheres, are color-coded on the basis of their R_{ex} values at 283 K. Color scheme: red for $R_{ex} > 10\ s^{-1}$, pink for $0\ s^{-1} < R_{ex} < 10\ s^{-1}$, and gray for residues whose dynamics data were not determined. This figure was prepared using MOLMOL (*38*).

Table 3: Inhibition by μ-SIIIA of Cloned Sodium Channels Expressed in *Xenopus* Oocytes[a]

sodium channel[b]	k_{on} (μM^{-1} min^{-1})	k_{off} (min^{-1})	IC_{50} (95% confidence interval) (μM)
$rNa_V1.1$	0.011 ± 0.004	0.2 ± 0.06	11(9.3−12.6)
$rNa_V1.2$	0.10 ± 0.015	irreversible[c]	NA[d]
$rNa_V1.3$	0.017 ± 0.002	0.12 ± 0.018	11(9.0−12.9)
$rNa_V1.4$	0.29 ± 0.036	0.04 ± 0.008	0.13(0.11−0.16)
$rNa_V1.5$	−[e]	−[e]	251 (204−308)[f]
$mNa_V1.6$	0.06 ± 0.012	0.082 ± 0.006	0.76(0.69−0.85)
$rNa_V1.7$	0.005 ± 0.0005	0.075 ± 0.012	65(57.8−73.1)

[a] Rate constants were determined as described in Experimental Procedures. The standard deviation and 95% confidence intervals were calculated from at least three independent experiments using Prism. [b] α-Subunit cloned from rat (r) or mouse (m). [c] Although the block was essentially irreversible within the experimental time frame, the k_{off} was estimated to be 0.0047 ± 0.0015 min^{-1} on the basis of residual recovery after 20 min of washing and assuming exponential decay. [d] Not available because slow kinetics precluded the steady state from being achieved within the experimental time frame. [e] Unable to be determined because block was too small and apparent kinetics too fast to be measured accurately. [f] Extrapolated value assuming 100% block at a saturating peptide concentration.

can be significantly affected by the anisotropic global reorientation of the molecule. However, in μ-SmIIIA, both Modelfree analysis and reduced spectral density mapping (which does not assume a particular model from rotational reorientation of the molecule) indicate that Cys4, Trp12, and Cys13 can undergo significant exchange on microsecond to millisecond time scales. It has been shown previously that the sign of dR_{ex}/dT indicates whether microscopic exchange

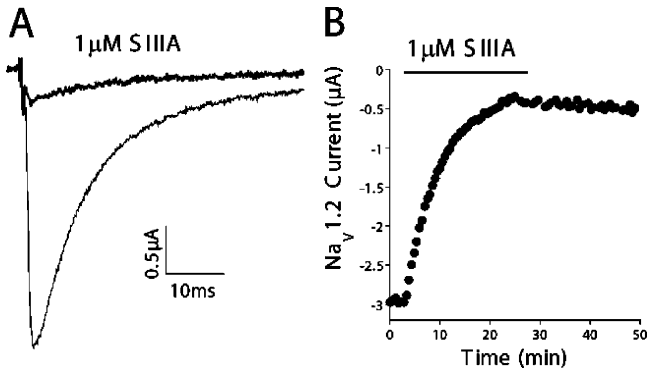

FIGURE 7: μ-SIIIA blocks rNa$_V$1.2 expressed in *Xenopus* oocytes. Oocytes were two-electrode voltage-clamped as described in Experimental Procedures. (A) Representative recordings, where each trace represents the average of five responses before (control, gray trace) and during (black trace) exposure to 1 μM μ-SIIIA. (B) Time course of block and recovery. The black bar above the plot indicates when μ-SIIIA was present.

is faster or slower than $3.2/\tau_{cp}$, where τ_{cp} is the interval between two consecutive 180° pulses in the CPMG segment of the pulse sequence used for $^{13}C^{\alpha}$ R_2 measurements (*48*). As one can see in Figure 5B, the magnitudes of R_{ex} for Cys4, Trp12, and Cys13 decrease with an increase in temperature. Thus, for a τ_{cp} of 900 μs for μ-SIIIA, an estimate of $k_{ex} > 3.2/\tau_{cp} = 3.6 \times 10^3$ s^{-1} can be obtained (*48*).

Given that Trp12 and Cys13 are adjacent to the biologically important Lys11, their observed propensity for conformational exchange implies that structural changes in this region may be possible upon binding to the sodium channel. As Lys11, Trp12, and Cys13 are part of the C-terminal helix, the conformation of this helix may also be subject to change upon sodium channel binding. Two of the residues exhibiting significant exchange, Cys4 and Cys13, are involved in disulfide bridges (although not to each other), raising the possibility that conformational transitions involving disulfide bonds may contribute to the observed exchange processes (*49*). The presence of conformational exchange and reduced order parameters in the loop between Cys8 and Cys13 is also not a simple function of loop size, as the least flexible region in the molecule is actually the longest loop, encompassed by Cys13 and Cys19.

The backbone dynamics of a ^{15}N-labeled ω-conotoxin MVIIA precursor have been studied previously using ^{15}N relaxation measurements (*27*). The backbone proved to be well-ordered on the nanosecond time scale, but residues 9−15 experienced conformational exchange processes with a time constant of ~35 μs. These observations were consistent with the results of ^{13}C relaxation measurements on unlabeled ω-MVIIA by Atkinson et al. (*50*), who detected conformational exchange in the loop between Cys8 and Cys15 and suggested that this was associated with conformational exchange of the Cys8−Cys20 disulfide bridge. As this region of the ω-conotoxins contains residues essential for Ca^{2+} channel binding (*51, 52*), it is possible that these exchange processes may influence activity.

Conclusions. The structure determined in this study for μ-SIIIA extends our understanding of the conformational space available to this class of conotoxins. Its well-defined C-terminal region closely matches the corresponding regions of all μ-conotoxins investigated to date, but its N-terminal half is distinct, sharing some features with the related

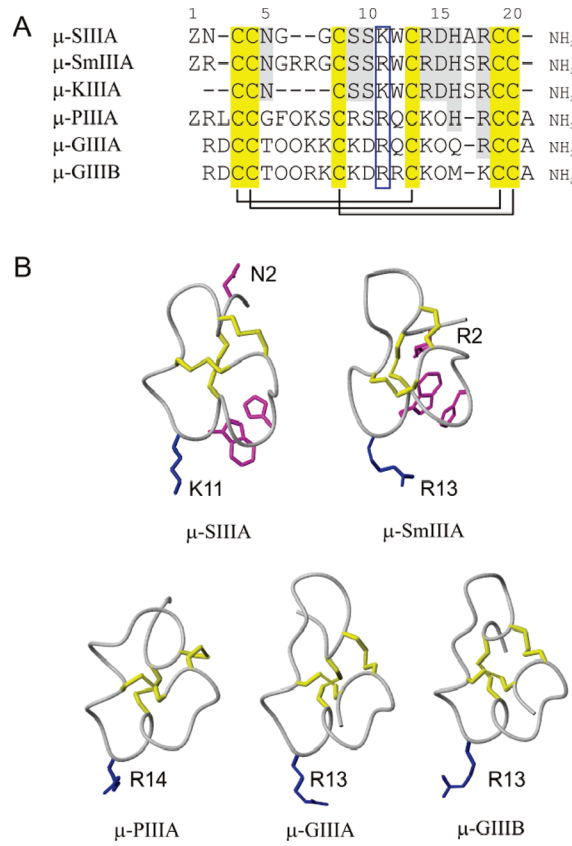

FIGURE 8: Sequence alignment and structure comparison of μ-conotoxins. (A) Amino acid sequences of μ-SIIIA, μ-SmIIIA, μ-PIIIA, μ-GIIIA, and μ-GIIIB. Numbers shown at the top are those for μ-SIIIA. Z represents pyroglutamate and O hydroxyproline. Conserved cysteines are highlighted in yellow and partially conserved residues in light gray. The Arg or Lys residues in the C-terminal half of the polypeptide (boxed in dark blue) have been suggested to play a key role in the potency of these peptides. (B) Structures of μ-SIIIA (BioMagResBank accession number 20023), μ-SmIIIA (PDB entry 1Q2J), μ-PIIIA (PDB entry 1R9I), μ-GIIIA (PDB entry 1TCJ), and μ-GIIIB (PDB entry 1GIB) with side chains of Arg or Lys colored dark blue and disulfide bonds colored yellow. All these structures are shown in a similar orientation after superimposition over backbone heavy atoms (C, C^{α}, and N) of aligned residues (Figure 8A); superposition over the C^{α} and C^{β} atoms of the six Cys residues gave a similar result. Side chains of Asn2, Trp12, and His16 of μ-SIIIA and Arg2, Trp14, and His18 of μ-SmIIIA are colored magenta. Panel B was generated using MOLMOL (*38*).

μ-conotoxin μ-SmIIIA but showing a more extended structure for the N-terminal residues. Internal motion of the backbone has been detected over various time scales, with pyroGlu1, Asn2, and Ser9 showing larger-magnitude motions on the picosecond to nanosecond time scale and Cys4, Trp12, and Cys13 undergoing conformational exchange on the microsecond to millisecond time scale. Even the presence of three disulfide bonds in a short polypeptide of just 20 residues is not sufficient to confer rigidity on the polypeptide backbone. Indeed, it may even be that conformational averaging associated with the disulfide bridges is the cause of the observed conformational exchange, as also suggested for ω-MVIIA (*50*). An awareness of the presence of conformational exchange is valuable in several ways. Interpreting measured NOEs as structural restraints requires some caution if either or both of the interacting nuclei are from regions undergoing such exchange. Knowing which regions of a structure are potentially flexible is also important if

modeling studies are to be undertaken on the basis of that structure, and most importantly of all, it must be taken into account when using structures determined in solution as a basis for understanding receptor binding or constructing mimetics (*53*). Whether conformational exchange serves any important biological function, for example, in allowing the toxin to undergo required conformational rearrangements as it engages its cognate binding site or whether it is simply an adventitious consequence of the presence of multiple disulfide bridges in certain environments remains to be established. One way of addressing this question is to replace some of the disulfide bridges with less flexible homologues, and means to achieve this are now available (*54*). In parallel with such efforts, greater access to backbone relaxation data afforded by high-field spectrometers equipped with more sensitive probes should contribute to an improved understanding of the relationships among structure, flexibility, and activity. Our results on the structure and dynamics of μ-SIIIA also provide a foundation for further structure−function studies on this therapeutically important group of conotoxins.

ACKNOWLEDGMENT

We thank Alex Morrison for his help with conopeptide synthesis, Alan Goldin for the clones for $Na_V1.1-1.6$, Gail Mandel for the $Na_V1.7$ clone, and Brian Smith, Chris MacRaild, and Jeff Babon for helpful discussions.

SUPPORTING INFORMATION AVAILABLE

NMR data and structure comparisons mentioned in the text. This material is available free of charge via the Internet at http://pubs.acs.org.

REFERENCES

1. Jones, R. M., and Bulaj, G. (2000) Conotoxins: New vistas for peptide therapeutics. *Curr. Pharm. Des. 6*, 1249–1285.
2. Norton, R. S., and Olivera, B. M. (2006) Conotoxins down under. *Toxicon 48*, 780–798.
3. Cestele, S., and Catterall, W. A. (2000) Molecular mechanisms of neurotoxin action on voltage-gated sodium channels. *Biochimie 82*, 883–892.
4. Catterall, W. A. (2000) From ionic currents to molecular mechanisms: The structure and function of voltage-gated sodium channels. *Neuron 26*, 13–25.
5. Goldin, A. L. (2001) Resurgence of sodium channel research. *Annu. Rev. Physiol. 63*, 871–894.
6. Cruz, L. J., Gray, W. R., Olivera, B. M., Zeikus, R. D., Kerr, L., Yoshikami, D., and Moczydlowski, E. (1985) *Conus geographus* toxins that discriminate between neuronal and muscle sodium channels. *J. Biol. Chem. 260*, 9280–9288.
7. Moczydlowski, E., Olivera, B. M., Gray, W. R., and Strichartz, G. R. (1986) Discrimination of muscle and neuronal Na-channel subtypes by binding competition between [^{3}H]saxitoxin and μ-conotoxins. *Proc. Natl. Acad. Sci. U.S.A. 83*, 5321–5325.
8. Safo, P., Rosenbaum, T., Shcherbatko, A., Choi, D. Y., Han, E., Toledo-Aral, J. J., Olivera, B. M., Brehm, P., and Mandel, G. (2000) Distinction among neuronal subtypes of voltage-activated sodium channels by μ-conotoxin PIIIA. *J. Neurosci. 20*, 76–80.
9. Li, R. A., Ennis, I. L., Xue, T., Nguyen, H. M., Tomaselli, G. F., Goldin, A. L., and Marban, E. (2003) Molecular basis of isoform-specific μ-conotoxin block of cardiac, skeletal muscle, and brain Na^+ channels. *J. Biol. Chem. 278*, 8717–8724.
10. Shon, K. J., Olivera, B. M., Watkins, M., Jacobsen, R. B., Gray, W. R., Floresca, C. Z., Cruz, L. J., Hillyard, D. R., Brink, A., Terlau, H., and Yoshikami, D. (1998) μ-Conotoxin PIIIA, a new peptide for discriminating among tetrodotoxin-sensitive Na channel subtypes. *J. Neurosci. 18*, 4473–4481.
11. Nielsen, K. J., Watson, M., Adams, D. J., Hammarstrom, A. K., Gage, P. W., Hill, J. M., Craik, D. J., Thomas, L., Adams, D., Alewood, P. F., and Lewis, R. J. (2002) Solution structure of μ-conotoxin PIIIA, a preferential inhibitor of persistent tetrodotoxin-sensitive sodium channels. *J. Biol. Chem. 277*, 27247–27255.
12. West, P. J., Bulaj, G., Garrett, J. E., Olivera, B. M., and Yoshikami, D. (2002) μ-conotoxin SmIIIA, a potent inhibitor of tetrodotoxin-resistant sodium channels in amphibian sympathetic and sensory neurons. *Biochemistry 41*, 15388–15393.
13. Keizer, D. W., West, P. J., Lee, E. F., Yoshikami, D., Olivera, B. M., Bulaj, G., and Norton, R. S. (2003) Structural basis for tetrodotoxin-resistant sodium channel binding by μ-conotoxin SmIIIA. *J. Biol. Chem. 278*, 46805–46813.
14. Bulaj, G., West, P. J., Garrett, J. E., Watkins, M., Zhang, M. M., Norton, R. S., Smith, B. J., Yoshikami, D., and Olivera, B. M. (2005) Novel conotoxins from *Conus striatus* and *Conus kinoshitai* selectively block TTX-resistant sodium channels. *Biochemistry 44*, 7259–7265.
15. Zhang, M. M., Green, B. R., Catlin, P., Fiedler, B., Azam, L., Chadwick, A., Terlau, H., McArthur, J. R., French, R. J., Gulyas, J., Rivier, J. E., Smith, B. J., Norton, R. S., Olivera, B. M., Yoshikami, D., and Bulaj, G. (2007) Structure/function characterization of μ-conotoxin KIIIA, an analgesic, nearly irreversible blocker of mammalian neuronal sodium channels. *J. Biol. Chem. 282*, 30699–30706.
16. Lewis, R. J., Schroeder, C. I., Ekberg, J., Nielsen, K. J., Loughnan, M., Thomas, L., Adams, D. A., Drinkwater, R., Adams, D. J., and Alewood, P. F. (2007) Isolation and structure-activity of μ-conotoxin TIIIA, a potent inhibitor of tetrodotoxin-sensitive voltage-gated sodium channels. *Mol. Pharmacol. 71*, 676–685.
17. Green, B. R., Catlin, P., Zhang, M. M., Fiedler, B., Bayudan, W., Morrison, A., Norton, R. S., Smith, B. J., Yoshikami, D., Olivera, B. M., and Bulaj, G. (2007) Conotoxins containing nonnatural backbone spacers: Cladistic-based design, chemical synthesis, and improved analgesic activity. *Chem. Biol. 14*, 399–407.
18. Lancelin, J. M., Kohda, D., Tate, S., Yanagawa, Y., Abe, T., Satake, M., and Inagaki, F. (1991) Tertiary structure of conotoxin GIIIA in aqueous solution. *Biochemistry 30*, 6908–6916.
19. Wakamatsu, K., Kohda, D., Hatanaka, H., Lancelin, J. M., Ishida, Y., Oya, M., Nakamura, H., Inagaki, F., and Sato, K. (1992) Structure-activity relationships of μ-conotoxin GIIIA: Structure determination of active and inactive sodium channel blocker peptides by NMR and simulated annealing calculations. *Biochemistry 31*, 12577–12584.
20. Hill, J. M., Alewood, P. F., and Craik, D. J. (1996) Three-dimensional solution structure of μ-conotoxin GIIIB, a specific blocker of skeletal muscle sodium channels. *Biochemistry 35*, 8824–8835.
21. Palmer, A. G. (1997) Probing molecular motion by NMR. *Curr. Opin. Struct. Biol. 7*, 732–737.
22. Fischer, M. W. F., Majumdar, A., and Zuiderweg, E. R. P. (1998) Protein NMR relaxation: Theory, applications and outlook. *Prog. Nucl. Magn. Reson. Spectrosc. 33*, 207–272.
23. Feher, V. A., and Cavanagh, J. (1999) Millisecond-timescale motions contribute to the function of the bacterial response regulator protein Spo0F. *Nature 400*, 289–293.
24. Volkman, B. F., Lipson, D., Wemmer, D. E., and Kern, D. (2001) Two-state allosteric behavior in a single-domain signaling protein. *Science 291*, 2429–2433.
25. Eisenmesser, E. Z., Bosco, D. A., Akke, M., and Kern, D. (2002) Enzyme dynamics during catalysis. *Science 295*, 1520–1523.
26. Frauenfelder, H., Parak, F., and Young, R. D. (1988) Conformational substates in proteins. *Annu. Rev. Biophys. Biophys. Chem. 17*, 451–479.
27. Goldenberg, D. P., Koehn, R. E., Gilbert, D. E., and Wagner, G. (2001) Solution structure and backbone dynamics of an ω-conotoxin precursor. *Protein Sci. 10*, 538–550.
28. Buczek, O., Wei, D., Babon, J. J., Yang, X., Fiedler, B., Chen, P., Yoshikami, D., Olivera, B. M., Bulaj, G., and Norton, R. S. (2007) Structure and sodium channel activity of an excitatory I_1-superfamily conotoxin. *Biochemistry 46*, 9929–9940.
29. Ellison, M., Feng, Z. P., Park, A. J., Zhang, X., Olivera, B. M., McIntosh, J. M., and Norton, R. S. (2008) α-RgIA, a novel conotoxin that blocks the α9α10 nAChR: Structure and identification of key receptor-binding residues. *J. Mol. Biol. 377*, 1216–1227.
30. Cornilescu, G., Delaglio, F., and Bax, A. (1999) Protein backbone angle restraints from searching a database for chemical shift and sequence homology. *J. Biomol. NMR 13*, 289–302.
31. Oldfield, E., Norton, R. S., and Allerhand, A. (1975) Studies of individual carbon sites of proteins in solution by natural abundance

carbon 13 nuclear magnetic resonance spectroscopy. Relaxation behavior. *J. Biol. Chem. 250*, 6368–6380.
32. Norton, R. S., Clouse, A. O., Addleman, R., and Allerhand, A. (1977) Studies of proteins in solution by natural-abundance carbon-13 nuclear magnetic resonance. Spectral resolution and relaxation behavior at high magnetic field strengths. *J. Am. Chem. Soc. 99*, 79–83.
33. Palmer, A. G., Cavanagh, J., Wright, P. E., and Rance, M. J. (1991) Sensitivity improvement in proton-detected 2-dimensional heteronuclear correlation NMR-spectroscopy. *J. Magn. Reson. 93*, 151–170.
34. Bartels, C., Xia, T., Billeter, M., Güntert, P., and Wüthrich, K. (1995) The program XEASY for computer-supported NMR spectral-analysis of biological macromolecules. *J. Biomol. NMR 6*, 1–10.
35. Herrmann, T., Güntert, P., and Wüthrich, K. (2002) Protein NMR structure determination with automated NOE assignment using the new software CANDID and the torsion angle dynamics algorithm DYANA. *J. Mol. Biol. 319*, 209–227.
36. Schwieters, C. D., Kuszewski, J. J., Tjandra, N., and Clore, G. M. (2003) The Xplor-NIH NMR molecular structure determination package. *J. Magn. Reson. 160*, 65–73.
37. Laskowski, R. A., Rullmannn, J. A., MacArthur, M. W., Kaptein, R., and Thornton, J. M. (1996) AQUA and PROCHECK-NMR: Programs for checking the quality of protein structures solved by NMR. *J. Biomol. NMR 8*, 477–486.
38. Koradi, R., Billeter, M., and Wüthrich, K. (1996) MOLMOL: A program for display and analysis of macromolecular structures. *J. Mol. Graphics 14*, 51–55, 29−32.
39. Ulrich, E. L., Akutsu, H., Doreleijers, J. F., Harano, Y., Ioannidis, Y. E., Lin, J., Livny, M., Mading, S., Maziuk, D., Miller, Z., Nakatani, E., Schulte, C. F., Tolmie, D. E., Kent Wenger, R., Yao, H., and Markley, J. L. (2008) BioMagResBank. *Nucleic Acids Res. 36*, D402–D408.
40. Farrow, N. A., Muhandiram, R., Singer, A. U., Pascal, S. M., Kay, C. M., Gish, G., Shoelson, S. E., Pawson, T., Forman-Kay, J. D., and Kay, L. E. (1994) Backbone dynamics of a free and a phosphopeptide-complexed Src homology-2 domain studied by ^{15}N NMR relaxation. *Biochemistry 33*, 5984–6003.
41. Mandel, A. M., Akke, M., and Palmer, A. G. (1995) Backbone dynamics of *Escherichia coli* ribonuclease Hi: Correlations with structure and function in an active enzyme. *J. Mol. Biol. 246*, 144–163.
42. Atkinson, R. A., and Lefevre, J. F. (1999) Reduced spectral density mapping for proteins: Validity for studies of ^{13}C relaxation. *J. Biomol. NMR 13*, 83–88.
43. Slupsky, C. M., Spyracopoulos, L., Booth, V. K., Sykes, B. D., and Crump, M. P. (2007) Probing nascent structures in peptides using natural abundance ^{13}C NMR relaxation and reduced spectral density mapping. *Proteins 67*, 18–30.
44. Wei, Y., Lee, D. K., and Ramamoorthy, A. (2001) Solid-state ^{13}C NMR chemical shift anisotropy tensors of polypeptides. *J. Am. Chem. Soc. 123*, 6118–6126.
45. Fiedler, B., Zhang, M. M., Buczek, O., Azam, L., Bulaj, G., Norton, R. S., Olivera, B. M., and Yoshikami, D. (2008) Specificity, affinity and efficacy of ι-conotoxin RXIA, an agonist of voltage-gated sodium channels $Na_V1.2$, 1.6 and 1.7. *Biochem. Pharmacol. 75*, 2334–2344.
46. Hyberts, S. G., Goldberg, M. S., Havel, T. F., and Wagner, G. (1992) The solution structure of eglin c based on measurements of many NOEs and coupling constants and its comparison with X-ray structures. *Protein Sci. 1*, 736–751.
47. Pallaghy, P. K., Duggan, B. M., Pennington, M. W., and Norton, R. S. (1993) Three-dimensional structure in solution of the calcium channel blocker ω-conotoxin. *J. Mol. Biol. 234*, 405–420.
48. Mandel, A. M., Akke, M., and Palmer, A. G., III (1996) Dynamics of ribonuclease H: Temperature dependence of motions on multiple time scales. *Biochemistry 35*, 16009–16023.
49. Otting, G., Liepinsh, E., and Wüthrich, K. (1993) Disulfide bond isomerization in BPTI and BPTI(G36S): An NMR study of correlated mobility in proteins. *Biochemistry 32*, 3571–3582.
50. Atkinson, R. A., Kieffer, B., Dejaegere, A., Sirockin, F., and Lefevre, J. F. (2000) Structural and dynamic characterization of ω-conotoxin MVIIA: The binding loop exhibits slow conformational exchange. *Biochemistry 39*, 3908–3919.
51. Norton, R. S., Pallaghy, P. K., Baell, J. B., Wright, C. E., Lew, M. J., and Angus, J. A. (1999) The polypeptide ω-conotoxin GVIA as a basis for new analgesic and neuroprotective agents. *Drug Dev. Res. 46*, 206–218.
52. Nielsen, K. J., Schroeder, T., and Lewis, R. (2000) Structure-activity relationships of ω-conotoxins at N-type voltage-sensitive calcium channels. *J. Mol. Recognit. 13*, 55–70.
53. Baell, J. B., Forsyth, S. A., Gable, R. W., Norton, R. S., and Mulder, R. J. (2001) Design and synthesis of type-III mimetics of ω-conotoxin GVIA. *J. Comput.-Aided Mol. Des. 15*, 1119–1136.
54. Robinson, A. J., Elaridi, J., Van Lierop, B. J., Mujcinovic, S., and Jackson, W. R. (2007) Microwave-assisted RCM for the synthesis of carbocyclic peptides. *J. Pept. Sci. 13*, 280–285.
55. Cho, C. H., Urquidi, J., Singh, S., and Robinson, G. W. (1999) Thermal offset viscosities of liquid H_2O, D_2O and T_2O. *J. Phys. Chem. B 103*, 1991–1994.

BI801010U